Dalton Transactions

PAPER

View Article Online
View Journal | View Issue



Cite this: *Dalton Trans.*, 2014, **43**, 15228

# Lattice defects and thermoelectric properties: the case of p-type $CuInTe_2$ chalcopyrite on introduction of zinc†

Jiangfeng Yang,[a,b] Shaoping Chen,*[a] Zhengliang Du,[b] Xianglian Liu[b] and Jiaolin Cui*[b]

Received 25th June 2014,
Accepted 29th July 2014

DOI: 10.1039/c4dt01909a

www.rsc.org/dalton

I–III–$VI_2$ chalcopyrites have unique inherent crystal structure defects, and hence are potential candidates for thermoelectric materials. Here, we identified mixed polyanionic/polycationic site defects ($Zn_{In}^{-}$, $V_{Cu}^{-}$, $In_{Cu}^{2+}$ and/or $Zn_{Cu}^{+}$) upon Zn substitution for either Cu or In or both in $CuInTe_2$, with the $Zn_{In}^{-}$ species originating from the preference of Zn for the cation 4b site. Because of the mutual reactions among these charged defects, Zn substitution in $CuInTe_2$ alters the basic conducting mechanism, and simultaneously changes the lattice structure. The alteration of the lattice structure can be embodied in an increased anion position displacement ($u$) or a reduced bond length difference ($\Delta d$) between $d_{(Cu-Te)4a}$ and $d_{(In-Te)4b}$ with increasing Zn content. Because of this, the lattice distortion is diminished and the lattice thermal conductivity ($\kappa_L$) is enhanced. The material with simultaneous Zn substitution for both Cu and In had a low $\kappa_L$, thereby we attained the highest $ZT$ value of 0.69 at 737 K, which is 1.65 times that of Zn-free $CuInTe_2$.

## 1. Introduction

Thermoelectric (TE) technology has great potential for directly converting waste heat into electricity, and hence it has attracted much attention in recent years. However, the relatively low efficiencies of current TE modules limit their large-scale commercialization. One issue is that three of the physical parameters that govern the TE performance, including the Seebeck coefficient ($\alpha$), electrical conductivity ($\sigma$) and thermal conductivity ($\kappa$), are interrelated, which makes it difficult to optimize them simultaneously. In order to improve the TE performance, we need to further explore new materials, such as chalcopyrites,[1] which usually have inherently low $\kappa$ and high $\alpha$ values. However, their electrical conductivities have to be improved.

$CuInTe_2$ (CIT) is a ternary I–III–$VI_2$ compound with a diamond-like structure (I = Cu, Ag; III = Al, Ga, In; VI = S, Se, Te). Its direct band gap ($E_g$) is approximately 1.02 eV.[2] Crystals of $CuInTe_2$ often show tetragonal distortion because $u \neq 0.25$, $\eta = c/2a \neq 1$ (here $u$ and $\eta$ are the anion position displacement parameters, and $a$ and $c$ are the lattice parameters), and the cation–anion distances are not equal ($d_{Cu-Te} \neq d_{In-Te}$).[3] Any occupation by foreign elements in the cation sites of $CuInTe_2$ will cause redistribution of the bond charges between Cu–Te and In–Te, thus leading to a tiny adjustment of the crystal structure.[4] In addition, upon occupation of impurity atoms (Me) in the cation sites, the simple conducting mechanisms will become more complicated due to the presence of donor–acceptor defect pairs ($2V_{Cu}^{-} + In_{Cu}^{2+}$)[3,5] and the potential creation/annihilation of these pairs, which modifies the physical properties. For example, in Mn-substituted $CuGaSe_2$, two anti-site defects ($Mn_{Cu}^{+}$ and $Mn_{Ga}^{-}$) are created.[6] The $Mn_{Cu}^{+}$ defect decreases the concentration of Cu vacancies ($V_{Cu}^{-}$), which thereby reduces the p-type carrier concentration. The effect of the p-type $Mn_{Ga}^{-}$ defect can neutralize that of the inherent $Ga_{Cu}^{2+}$ defect, so that the material exhibits ferromagnetic behavior.[6] In Mn-substituted $CuInTe_2$, samples with 3% Mn substitution in the Cu sites are paramagnetic, but samples with higher Mn concentration (9% < $x$ < 12%) exhibit antiferromagnetic coupling.[7] Moreover, the site preferences of some elements in ternary I–III–$VI_2$ compounds could lead to the formation of unexpected functional units. For instance, in Mn-substituted $CuInSe_2$, Mn prefers the Cu sites,[8] or the In sites under Cu-rich and In-poor conditions,[9] which helps form the $Mn_{Cu}^{+}$ or $Mn_{In}^{-}$ anti-site defects. The formation of $Mn_{Cu}^{+}$ can help create the electrically conducting unit Mn–Se,[10] thus enhancing the electrical conductivity of $CuInSe_2$.

[a]*Materials Science and Engineering College, Taiyuan University of Technology, Taiyuan 030024, China*
[b]*Institute of Materials Engineering, School of Materials, Ningbo University of Technology, Ningbo 315016, China. E-mail: cuijiaolin@163.com*
†Electronic supplementary information (ESI) available. See DOI: 10.1039/c4dt01909a

Since Zn has an electronegativity of 1.65, smaller than those of In (1.78) or Cu (1.9), we believe that upon the addition of Zn to CIT, Zn will occupy the cation (In or Cu) sites, rather than the anion (Te) sites. Such occupations favour the formation of slab ZnTe, which reduces the Te p–Cu d repulsion near the upper valence band (VBM)[11] and causes a splitting of the valence band into two sub-bands due to the band-anticrossing effect (BAC).[12] This effect was also observed when Cu was introduced into $As_2Se_3$[13] and when oxygen was introduced into ZnSe.[14,15] In light of this, the band gap narrows due to the appearance of extended states or impurity levels in the mid-gap region, thus increasing the Seebeck coefficient.[15]

In this work, we identified multiple anti-site defects ($Zn_{In}^{-}$, $V_{Cu}^{-}$, $In_{Cu}^{2+}$ and/or $Zn_{Cu}^{+}$) *via* the substitution of Zn for either Cu or In or both in $CuInTe_2$. Such substitutions alter the basic conducting mechanism and lattice structure, tuning the TE performance of $CuInTe_2$.

## 2. Experimental

### Sample preparation

Three sorts of compounds, $Cu_{1-x}In_{1-x}Zn_{2x}Te_2$ (CI-poor), $CuIn_{1-x}Zn_xTe_2$ (In-poor) and $Cu_{1-x}InZn_xTe_2$ (Cu-poor) ($x$ = 0, 0.02, 0.05, 0.1, 0.2), were synthesized in evacuated silica tubes *via* high temperature solid-state reactions of the four elements (Cu, In, Te and Zn) with 5 N purity at 1373 K for 24 h in a programmable furnace. The melts were then slowly cooled to 650 °C, and were kept at this temperature for 240 h in vacuum. Subsequently, the ingots were cooled to room temperature (RT) in the furnace. Such a synthesis process assures near-equilibrium chemical compositions, or that only a chalcopyrite-type structure will be obtained without phase transitions.[16]

The as-solidified ingots were pulverized and then ball-milled in stainless steel bowls containing benzinum, at a rotation rate of 350 rpm for 5 h. The dried powders were quickly sintered using a spark plasma sintering apparatus (SPS-1030) with a designed sintering program under a pressure of 50 MPa. The densities of the sintered samples were measured using Archimedes' method. The sintered blocks with size of ∅ 20 mm × 2.5 mm were cut into 3 mm thick slices measuring 2.5 mm × 12 mm for the electrical property measurements.

### Physical measurements

The Seebeck coefficients ($\alpha$) and electrical conductivities ($\sigma$) were measured as a function of temperature using an ULVAC ZEM-2 instrument system in a helium atmosphere between RT and 740 K. A temperature difference of approximately 5 °C was applied between the two terminals of the sample in order to measure the Seebeck coefficient, whereas the electrical conductivity was measured using the four-probe method. According to several repeated measurements on the same samples, it is clear that the corrected data are of good accuracy, with errors of below 10.0% for both the Seebeck coefficients and the electrical conductivities. The thermal conductivities ($\kappa$) at RT ~ 735 K were calculated as the products of the material densities, thermal diffusivities (with errors of below 10.0%) and specific heats (with errors of below 6.0%) measured by a laser flash method (TC-1200RH apparatus). The Hall coefficient ($R_h$) measurements at RT were conducted on a Physical Property Measurement System (PPMS, Model-9) using a four-probe configuration with a magnetic field sweeping between ±1.0 T, and were performed on rectangular samples with size 2 × 2 × 8 $cm^3$. The Hall mobilities ($\mu$) and carrier concentrations ($n$) were subsequently calculated from the relations $\mu = R_h\sigma$ and $n = 1/(eR_h)$ respectively, where $e$ is the electron charge. The current and Hall voltage leads were fine copper wires, and the contacts were made of silver paste. The absorption coefficient measurements were carried out using a Perkin-Elmer Lambda 950 UV-VIS-NIR spectrophotometer, and absorption spectra for the powders were recorded between the visible and infrared regions (200–900 nm).[17]

### Structural analysis

The structural analysis of the powders was carried out using a powder X-ray diffractometer (D8 Advance) operating at 50 kV and 40 mA, using Cu Kα radiation ($\lambda$ = 0.15406 nm) and a scan rate of 4° $min^{-1}$ over a range from 10° to 100°. Rietveld refinements for X-ray powder diffraction (XRPD) were performed using FULLPROF, and the X-ray diffraction peak shapes were quantified using a Pseudo–Voigt function and a Pseudo-Voigt function with the Finger–Cox–Jephcoat asymmetry correction. The background was described as a shifted Chebyshev type. In chalcopyrite-type $CuInTe_2$, there are two cation sites, Cu on site 4a (0, 0, 0) and In on site 4b (0, 0, 0.5). The anionic Te atoms on site 8d ($x_{Te}$, 0.25, 0.125 with $x_{Te}$ ~ 0.25) are coordinated by two Cu and two In cations. The following parameters were refined: lattice parameters, peak shape parameters, atomic coordinates, isotropic displacement parameters ($U_{iso}$) and site occupation factors (SOFs). Each structural model was refined to convergence.

### Band structure and formation energy calculations

The *ab initio* calculations were performed using the plane-wave pseudopotential technique with CASTEP software[18] based on density functional theory (DFT). The generalized gradient approximation (GGA)[19] was used, and the Perdew, Burke, Ernzerhof (PBE) functional was adopted for the exchange–correlation energy. We used the norm-conserving pseudopotential with a cutoff energy of 500 eV and a $k$ mesh of 4 × 4 × 2 for geometry optimizations. $3d^{10}4s^1$, $5s^25p^1$, and $5s^25p^4$ were treated as the valence states of Cu, In, and Te respectively. In the geometrical optimizations, all forces on atoms converged to less than 0.03 eV $Å^{-1}$. The maximum ionic displacement was confined to within 1 × $10^{-3}$ Å, and the total stress tensor was reduced to the order of 0.05 GPa.

We used four formula units per conventional cell for the model, which was composed of four Cu, four In and eight Te atoms. We assumed that the structure was retained on doping, but that Zn was arranged in the Cu or In or both lattice sites,

corresponding to Zn occupations of 25.0 at% in the Cu and In lattice sites.

When calculating the formation energies, we also used the generalized gradient approximation (GGA), but with a cutoff energy of 400 eV and a $k$ mesh of $4 \times 4 \times 3$.

### X-ray photoelectron spectroscopy

X-ray photoelectron spectroscopy (XPS) measurements were performed on an AXIS ULTRA DLD equipped with a monochromatic Al Kα X-ray source (30 mA, 15 kV) and a hybrid lens. Samples were sputter-cleaned with an Art ion beam until the core-line peaks associated with surface oxides were no longer observed in the XPS spectra. High-resolution core-line spectra of $Zn2p_{3/2}$, $Cu2p_{3/2}$, $In3d_{5/2}$, and $Te3p_{5/2}$ were collected. Because of the low concentration of Zn in the Cu(In)- and CI-poor compounds, only three Zn-rich members ($Cu_{0.9}In_{0.9}Zn_{0.2}Te_2$, $Cu_{0.9}InZn_{0.1}Te_2$ and $CuIn_{0.9}Zn_{0.1}Te_2$) were examined. $CuInTe_2$ was examined for comparison.

## 3. Results and discussion

X-ray diffraction patterns for three kinds of samples are shown in Fig. S1.† No visible impurity phases were identified at $x < 0.2$. This indicates that almost all Zn atoms were incorporated into the crystal lattice, and that the materials crystallize in a single chalcopyrite structure (PDF 34-1498). At $x = 0.2$, a minor ZnTe phase (PDF 19-1482) was identified in the In(Cu)-poor systems, therefore we stopped investigating the materials with $x > 0.2$.

The band structure of CIT and its density of states (DOS) are presented in Fig. S2(a and b†), in which a direct band gap was observed ($E_g$ = 1.09 eV). The Fermi level ($E_F$) lies in the valence band maximum (VBM). When Zn atoms (25.0 at%) occupy Cu and In sites simultaneously, the $E_g$ value gets smaller ($E_g$ = 0.75 eV), and a relatively flat band compared with that of CIT was observed near the $E_F$ (see Fig. S2c and d†), suggesting that there is a potential increase in the effective mass of the valence band. When Zn atoms (25.0 at%) settle in the Cu sites only, the $E_F$ moves to the conduction band, with $E_g$ = 0.95 eV, as shown in Fig. S3(a and b†), suggesting that the material exhibits n-type conduction. However, $E_F$ drops to the valence band, with $E_g$ = 0.30 eV, when Zn settles in the In sites (25.0 at%) (Fig. S3c and d†). Such a significant reduction in the band gap, $E_g$, upon Zn occupation in the In sites seems to be caused by the ZnTe impurity level just above the VBM (red line in Fig. S3c†), which enters the mid-gap region.[12,15] However, we did not observe the so-called impurity-induced peak caused by the BAC effect in the density of states (DOS),[12] even though there is a relatively high DOS near the Fermi level, as shown in Fig. S3d.†

The above calculations reveal that the different Zn occupations have different effects on the band structure. However, in the actual materials we only observed a slight widening of the band gap compared with Zn-free CIT, upon Zn substitution. The $E_g$ value remains almost unchanged (0.8–0.85 eV) in the three Zn-substituted materials, regardless of the Zn content (see Fig. S4a–c†). This implies that, in the actual materials, the creation of defects due to the introduction of Zn is not as simple as we anticipated. There must be multiple anti-site defects, each of which plays its own role.

In order to determine the exact locations of Zn and the anti-site defects in the real Zn-substituted CIT materials, we calculated the formation energies when Zn occupies either Cu or In or both sites, based on the following reactions:

$$Cu_4In_4Te_8 + Zn = Cu_4In_3ZnTe_8 + In \quad \text{(occupying In lattice sites)} \tag{1}$$

$$Cu_4In_4Te_8 + Zn = Cu_3ZnIn_4Te_8 + Cu \quad \text{(occupying Cu lattice sites)} \tag{2}$$

$$Cu_4In_4Te_8 + 2Zn = Cu_3In_3Zn_2Te_8 + Cu + In \quad \text{(occupying both Cu and In lattice sites)} \tag{3}$$

Then, we obtain:

$$E_f = E_f(Cu_4In_3ZnTe_8) + E_T(In) - E_T(Cu_4In_4Te_8) - E_T(Zn) \tag{4}$$

$$E_f = E_f(Cu_3ZnIn_4Te_8) + E_T(Cu) - E_T(Cu_4In_4Te_8) - E_T(Zn) \tag{5}$$

$$E_f = E_f(Cu_3In_3Zn_2Te_8) + E_T(Cu) + E_T(In) - E_T(Cu_4In_4Te_8) - 2E_T(Zn) \tag{6}$$

where $E_f$ is the formation energy and $E_T$ is the total energy of each material.

The results reveal that the formation energies ($E_f$) are −5.943 eV, −4.549 eV and −2.184 eV, corresponding to Zn occupation in the In, Cu and both lattice sites, respectively. This suggests that Zn has a preference for the In sites rather than the Cu sites, and that simultaneous Zn occupation in both the Cu and In sites is the least probable.

To further confirm the site preferences of Zn, we calculated the SOFs for the CI-poor and the Cu(In)-poor systems using Rietveld refinement, according to the two models proposed below:

$$\text{Model A: } (Cu, In, Zn)_{4a}(In, Cu, Zn)_{4b}(Te_{2-\delta})_{8d}$$

$$\text{Model B: } (In, Zn)_{4a}(In, Cu, Zn)_{4b}(Te_{2-\delta})_{8d}$$

In model A, the cation sites (4a and 4b) are proposed to be occupied by Cu, Zn, and In ions simultaneously, while in model B, the 4a sites are only occupied by In and Zn ions.

For model A,

$$SOF(Cu)_{4a} + SOF(Zn)_{4a} + SOF(In)_{4a} = 1 \tag{7}$$

$$SOF(Cu)_{4b} + SOF(Zn)_{4b} + SOF(In)_{4b} = 1 \tag{8}$$

$$SOF(Zn)_{4a} + SOF(Zn)_{4b} = 0.02, 0.05 \text{ and } 0.1 \tag{9}$$

For model B,

$$SOF(In)_{4a} + SOF(Zn)_{4a} = 1 \tag{10}$$

 

$$\mathrm{SOF(Cu)_{4b}} + \mathrm{SOF(Zn)_{4b}} + \mathrm{SOF(In)_{4b}} = 1 \quad (11)$$

$$\mathrm{SOF(Zn)_{4a}} + \mathrm{SOF(Zn)_{4b}} = 0.02, 0.05 \text{ and } 0.1 \quad (12)$$

The final results obtained using model B for the sample with $x$ = 0.1 are shown in Table 1. The preliminary fitting results are presented in Tables SI–III and Fig. S5.† We observed that Zn has a preference for the In sites rather than the Cu sites in all three materials, which is in accordance with the results obtained from the formation energy calculations. Besides, Cu is unlikely to occupy the In sites, and indium has an increasing tendency to occupy the Cu sites as the Zn content increases, which is specified in model B.

Because of the site preference of Zn, a large number of $Zn_{In}^{-}$ site defects are present in the materials. However, we cannot rule out the $Zn_{Cu}^{+}$ and $In_{Cu}^{2+}$ defects originating from the occupation of Zn and expelled In ions in the Cu sites. The creation of such defects could reduce the number of inherent Cu vacancies ($V_{Cu}^{-}$) in CIT and disturb the original Coulombic attraction between $In_{Cu}^{2+}$ and $2V_{Cu}^{-}$.[20] As a consequence, there must be mixed polyanionic/polycationic species present in Zn-substituted CIT, with each making its own contributions.

In order to confirm the presence of the species ($Zn_{In}^{-}$, $Zn_{Cu}^{+}$ and $In_{Cu}^{2+}$), we determined the oxidation states of Cu, Zn and In using Cu2p, Zn2p and In3d XPS spectra; the results are shown in Fig. 1. The average binding energy (BE) values with uncertainties estimated at ~±0.01 eV are listed in Table 2, in which we observed that the BE values of $Zn2p_{3/2}$ (1021.8–1022.0 eV) are all higher than that of elemental Zn (1021.45 eV), but very close to that of ZnTe.[21] We therefore confirmed the presence of ionic $Zn^{2+}$. On the other hand, the absence of a satellite (at 940–945 eV) above the $2p_{3/2}$ core-line peak in the Cu2p spectrum (see Fig. 1) and the resemblance of the Cu2p spectrum to that reported in ref. 10 and those of the copper(I) halides (*e.g.* CuBr, CuI)[22] can confirm the presence of

**Table 1** Structural parameters and refinement details for the CI-poor, Cu-poor and In-poor compounds ($x$ = 0.1) obtained from Rietveld refinements

| Parameters | CI-poor Model B | Cu-poor Model B | In-poor Model B |
|---|---|---|---|
| Cation 4a | | | |
| SOF(Cu) | 0.9000 | 0.9000 | 1.0000 |
| SOF(In) | 0.1297 | 0.1615 | 0.0891 |
| SOF(Zn) | 0.0297 | −0.0615 | 0.0891 |
| $100U_{iso}$ (Å$^2$) | 1.0950 | 1.4010 | 1.1720 |
| Cation 4b | | | |
| SOF(In) | 0.8448 | 0.9090 | 0.8997 |
| SOF(Cu) | 0.0000 | 0.0000 | 0.0000 |
| SOF(Zn) | 0.1552 | 0.0910 | 0.1003 |
| $100U_{iso}$ (Å$^2$) | 2.0490 | 1.5530 | 2.3910 |
| Anion 8d | | | |
| SOF(Te) | 1.0044 | 0.9929 | 0.9997 |
| $100U_{iso}$ (Å$^2$) | 2.1460 | 1.9780 | 2.1100 |
| $x_{Te}$ | 0.2312 | 0.2299 | 0.2269 |
| Reliability factors | | | |
| $\chi^2$ | 1.570 | 1.6290 | 1.9870 |
| w$R_p$ | 0.0883 | 0.0887 | 0.0999 |
| $R_p$ | 0.0681 | 0.0688 | 0.0767 |

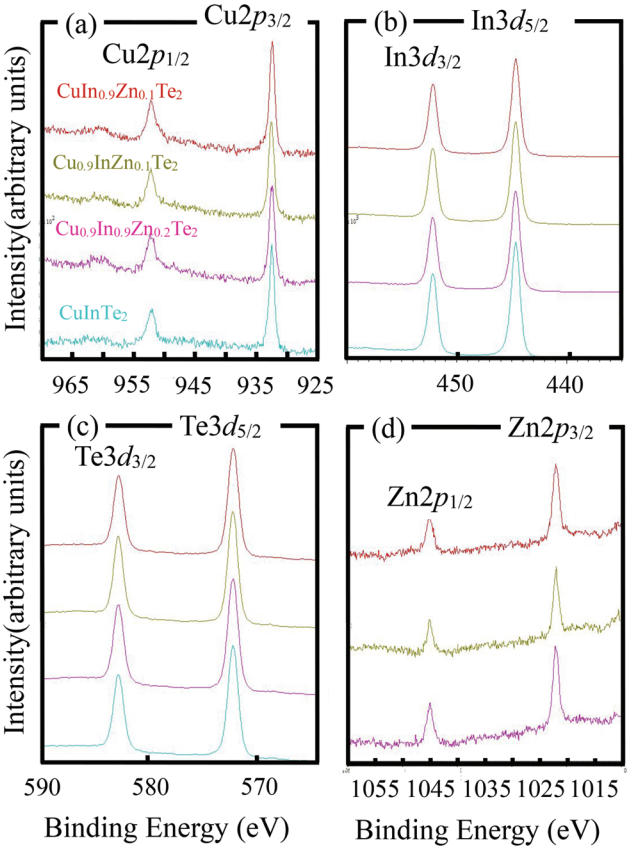


**Fig. 1** XPS spectra of (a) Cu2p, (b) In3d, (c) Te3d, and (d) Zn2p for $CuInTe_2$, $Cu_{0.9}In_{0.9}Zn_{0.2}Te_2$, $Cu_{0.9}InZn_{0.1}Te_2$, and $CuIn_{0.9}Zn_{0.1}Te_2$.

**Table 2** Binding energies from the $Zn2p_{3/2}$, $Cu2p_{3/2}$, $In3d_{5/2}$, and $Te3d_{5/2}$ core-level photoelectron spectra for the $CuInTe_2$, $Cu_{0.9}In_{0.9}Zn_{0.2}Te_2$, $Cu_{0.9}InZn_{0.1}Te_2$ and $CuIn_{0.9}Zn_{0.1}Te_2$ compounds

| Compounds | $Zn2p_{3/2}$ (eV) | $Cu2p_{3/2}$ (eV) | $In3d_{5/2}$ (eV) | $Te3d_{5/2}$ (eV) |
|---|---|---|---|---|
| $CuInTe_2$ | | 932.5 | 444.6 | 572.6 |
| $Cu_{0.9}In_{0.9}Zn_{0.2}Te_2$ | 1022.0 | 932.4 | 444.6 | 572.6 |
| $Cu_{0.9}InZn_{0.1}Te_2$ | 1021.8 | 932.6 | 444.6 | 572.7 |
| $CuIn_{0.9}Zn_{0.1}Te_2$ | 1021.9 | 932.4 | 444.6 | 572.6 |

$Cu^{+}$. In addition, the $In3d_{5/2}$ BE (444.6 eV) in the three materials is higher than that of elemental In (443.8 eV), but almost equal to those of $In_2O_3$ (444.7 eV) and $In_2Se_3$ (444.6 eV),[21] which indicates the presence of positively charged $In^{3+}$ species. Therefore, the formation of $Zn_{Cu}^{+}$ and $Zn_{In}^{-}$ anti-site defects upon Zn substitution in the Cu or In sites can be confirmed. The formation of $In_{Cu}^{2+}$ is attributed to the occupation by expelled In ions in the Cu sites, as mentioned above. A schematic model of the cell formed upon creation of these defects in $CuInTe_2$ chalcopyrite is shown in Fig. S6.†

The creation of the $Zn_{In}^{-}$ ($Zn_{Cu}^{+}$) defect drops (moves) the $E_F$ into the acceptor (donor) level, which might narrow (widen) the band gap (see Fig. S3†), while the reduction[4b] or creation[23] of $V_{Cu}^{-}$ could conserve or increase the band gap in Cu–Ga(In)–

$Te(Se)_2$ systems. This is why we did not observe a visible change in the band gap in the three sorts of materials. On the other hand, the response of each species to the carrier concentration, $n$, is also different. Some species acts as donors, while others act as acceptors. The detailed responses are estimated and summarized in Table 3. Taken together, the p-type carrier concentration ($n$) in the CI-poor system has a tendency to increase, while those in the In- and Cu-poor systems show a tendency to decrease. In order to verify these estimations, we measured the Hall coefficients ($R_h$) and carrier concentrations ($n$) at RT, and found that the $n$ value in the CI-poor system increases from $7.74 \times 10^{25}$ ($x$ = 0.02) to $9.65 \times 10^{25}$ $m^{-3}$ ($x$ = 0.1), which is more than one order of magnitude higher than that in Zn-free CIT ($2.65 \times 10^{24}$ $m^{-3}$).[1d] The $n$ value in the In (Cu)-poor system decreases from 2.86 (11.90) $\times 10^{24}$ ($x$ = 0.02) to 2.33 (7.79) $\times 10^{24}$ $m^{-3}$ ($x$ = 0.1) (see Table 4), thus clearly confirming the estimations shown in Table 3. However, the carrier concentrations in the In- or Cu-poor system are approximately one to two orders of magnitude smaller than the optimal one ($10^{25}$ to $10^{26}$ $m^{-3}$),[24] which implies that there is still much room for improvement in the TE performance.

The TE properties of the CI-poor system are presented in Fig. 2, in which we observed that the Seebeck coefficient ($\alpha$) at $x > 0.02$ increases with temperature over the measured temperature range, but gradually decreases with increasing Zn content (Fig. 2a). Although the $\alpha$ values are lower than those of CIT when $T < 670$ K, they gradually approach the values for CIT at $T > 700$ K. The maximum $\alpha$ value ($x$ = 0.02) is 212.0 μV $K^{-1}$ at 737 K. The electrical conductivity ($\sigma$), which is much higher than that of Zn-free CIT, decreases with increasing temperature (Fig. 2b). At 737 K, the $\sigma$ value ($x$ = 0.02) is $2.16 \times 10^4$ $\Omega^{-1}$ $m^{-1}$, increasing by a factor of about 1.5 compared with Zn-free CIT. In addition, the CI-poor system has a much lower $\kappa_L$ value (~0.65 W $K^{-1}$ $m^{-1}$) when $x < 0.05$ at 737 K, however

**Table 3** Formation of cations (anions) and estimated changes in the carrier concentration ($n$) in different Zn-substituted $CuInTe_2$ materials

| Possible formation of defects | Conducting type | Estimated carrier concentration ($n$) | Estimated change in $n$ with $x$ |
|---|---|---|---|
| $Cu_{1-x}In_{1-x}Zn_{2x}Te_2$ (CI-poor) | | | |
| $Zn_{In}^-$ | Acceptor | A large quantity | Increase with increasing $x$ |
| $V_{Cu}^-$ | Acceptor | A relatively large quantity | Increase with increasing $x$ |
| $Zn_{Cu}^+$ | Donor | A small quantity | No significant change |
| $In_{Cu}^{2+}$ | Donor | A small quantity | Increase with increasing $x$ |
| Taken together, p-type carrier concentration ($n$) in CI-poor | | | Tendency to increase |
| $CuIn_{1-x}Zn_xTe_2$ (In-poor) | | | |
| $Zn_{In}^-$ | Acceptor | A large quantity | Increase with increasing $x$ |
| $V_{Cu}^-$ | Acceptor | A limited quantity | Decrease with increasing $x$ |
| $Zn_{Cu}^+$ | Donor | — | — |
| $In_{Cu}^{2+}$ | Donor | A small quantity | Increase with increasing $x$ |
| Taken together, p-type carrier concentration ($n$) in In-poor | | | Tendency to decrease |
| $Cu_{1-x}InZn_xTe_2$ (Cu-poor) | | | |
| $Zn_{In}^-$ | Acceptor | A large quantity | Increase with increasing $x$ |
| $V_{Cu}^-$ | Acceptor | A large quantity | Relative increase with increasing $x$ |
| $Zn_{Cu}^+$ | Donor | A certain quantity | Increase with increasing $x$ |
| $In_{Cu}^{2+}$ | Donor | A small quantity | Significant increase with increasing $x$ |
| Taken together, p-type carrier concentration ($n$) in Cu-poor | | | Tendency to decrease |

**Table 4** Solid state parameters of solid solutions of the $CuInTe_2$-based compounds measured at RT

| Samples | Hall coefficient, $R_h$ ($m^3$ $C^{-1}$) | Carrier concentration, $n$ ($m^{-3}$) | Mobility, $\mu$ ($m^2$ $V^{-1}$ $s^{-1}$) | Electrical conductivity, $\sigma$ ($W^{-1}$ $m^{-1}$) | Seebeck coefficient, $\alpha$ (μV $K^{-1}$) | Effective mass, $m^*$ | $u$ | $\eta$ |
|---|---|---|---|---|---|---|---|---|
| $CuInTe_2$ (CIT) | | | | | | | | |
| | $2.36 \times 10^{-6}$ | $2.65 \times 10^{24}$ | $5.48 \times 10^{-3}$ | $2.32 \times 10^3$ | 181.98 | 0.16 | 0.2482 | 1.0035 |
| $Cu_{1-x}In_{1-x}Zn_{2x}Te_2$ (CI-poor) | | | | | | | | |
| $x$ = 0.02 | $8.08 \times 10^{-8}$ | $7.74 \times 10^{25}$ | $3.64 \times 10^{-3}$ | $4.32 \times 10^4$ | 129.03 | 1.09 | 0.2482 | 1.0036 |
| $x$ = 0.05 | | | N/A | | | | 0.2484 | 1.0031 |
| $x$ = 0.1 | $6.48 \times 10^{-8}$ | $9.65 \times 10^{25}$ | $2.27 \times 10^{-3}$ | $3.48 \times 10^4$ | 105.34 | 1.03 | 0.2485 | 1.0029 |
| $CuIn_{1-x}Zn_xTe_2$ (In-poor) | | | | | | | | |
| $x$ = 0.02 | $2.19 \times 10^{-6}$ | $2.86 \times 10^{24}$ | $6.90 \times 10^{-2}$ | $3.09 \times 10^4$ | 145.12 | 0.13 | 0.2482 | 1.0035 |
| $x$ = 0.05 | | | N/A | | | | 0.2483 | 1.0033 |
| $x$ = 0.1 | $2.68 \times 10^{-6}$ | $2.33 \times 10^{24}$ | $1.76 \times 10^{-1}$ | $6.41 \times 10^4$ | 105.23 | 0.09 | 0.2485 | 1.0030 |
| $Cu_{1-x}InZn_xTe_2$ (Cu-poor) | | | | | | | | |
| $x$ = 0.02 | $5.24 \times 10^{-7}$ | $1.19 \times 10^{25}$ | $2.37 \times 10^{-2}$ | $4.54 \times 10^4$ | 131.72 | 0.32 | 0.2481 | 1.0037 |
| $x$ = 0.05 | | | N/A | | | | 0.2483 | 1.0035 |
| $x$ = 0.1 | $8.03 \times 10^{-7}$ | $7.79 \times 10^{24}$ | $4.93 \times 10^{-2}$ | $6.13 \times 10^4$ | 92.53 | 0.17 | 0.2483 | 1.0034 |

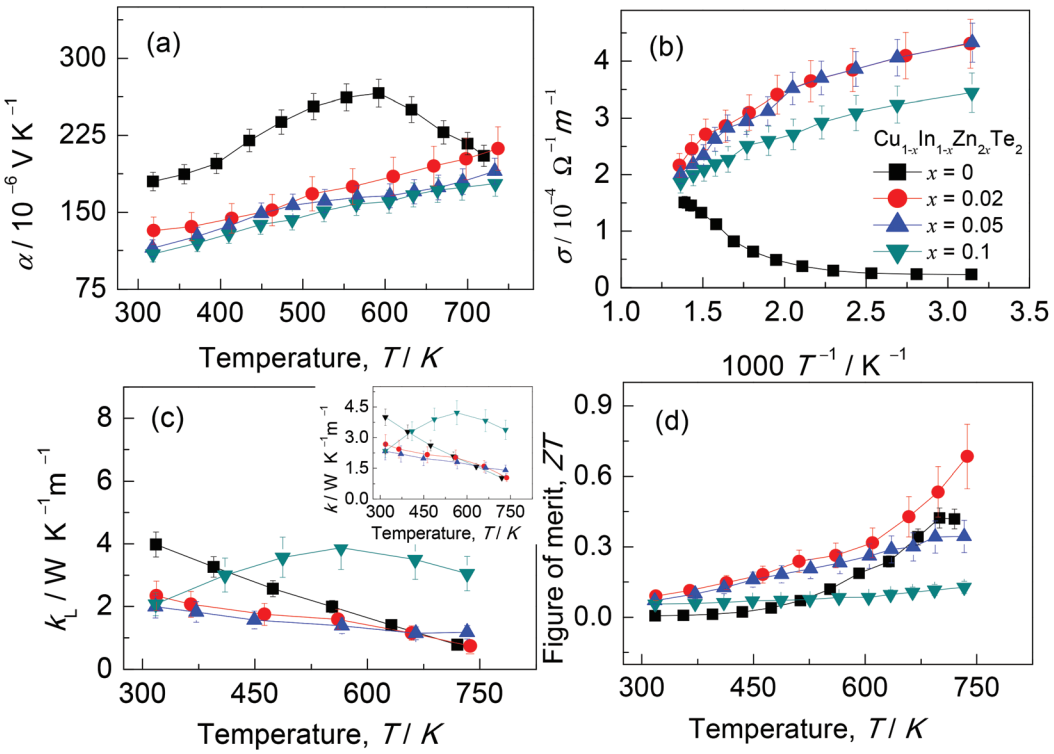


**Fig. 2** Thermoelectric properties of $Cu_{1-x}In_{1-x}Zn_{2x}Te_2$: (a) Seebeck coefficients ($\alpha$), (b) electrical conductivities ($\sigma$), (c) lattice thermal conductivities ($\kappa_L$) (the inset shows the relationship between $\kappa$ and $T$), and (d) $ZT$ values.

this value shows a tendency to increase with increasing Zn content above 650 K. At $x = 0.1$, the $\kappa_L$ value reaches ~3.05 W $K^{-1}$ $m^{-1}$ at 737 K (Fig. 2c); the inset in Fig. 2c shows the total $\kappa(T)$, which exhibits almost the same temperature dependence as $\kappa_L$. Combining the three parameters, we attained the highest $ZT$ value of 0.69 at 737 K when $x = 0.02$ (Fig. 2d), an increase by a factor of 1.65 compared with Zn-free CIT. The $ZT$ value is much higher than those of $CuInTe_2$ ($ZT$ = 0.27–0.5 at 600–710 K)[1d–f] and $Zn_{0.03}Cu_{0.97}FeS_2$ ($ZT$ = 0.04 at 400 K),[25] and it is comparable to that of $Ag_{0.95}GaTe_2$ ($ZT$ = 0.77 at 850 K).[1c] However, it is much lower than that of $CuGaTe_2$[1a] ($ZT$ = 1.45 at 940 K) and that reported for $CuInTe_2$ at 850 K ($ZT$ = 1.18).[1b]

In the In and Cu-poor systems, the temperature dependencies of both $\alpha$ and $\sigma$ are also quite different from those of CIT, as shown in Fig. 3a and b and Fig. 4a and b. However, the temperature dependence of the Seebeck coefficient is similar for each Zn concentration. The reason is that the effective masses ($m^*$) and carrier concentrations ($n$) are optimized, according to the relation: $\alpha = \frac{8\pi^2\kappa_B^2 T}{3eh^2} m^* \left(\frac{\pi}{3n}\right)^{\frac{2}{3}}$,[26] as shown in Table 4. In addition, the $\sigma$ value increases with increasing Zn content in both systems. Relatively high electrical conductivities in the In(Cu)-poor systems might be due to the fact that widening of the band gap prevents thermal activation of the minority carriers at high temperatures,[27] rather than due to the introduction of the impurity level, which narrows the band gap and then facilitates the thermal activation of electrons from the conduction band.[28] Moreover, the two sorts of materials have high $\kappa_L$ values compared with their CI-poor counterparts, and these values show a tendency to increase with increasing Zn content above ~550 K (see Fig. 3c and Fig. 4c; the insets show the total $\kappa(T)$). Therefore, we could only attain limited $ZT$ values (0.34 (0.43) at $x = 0.02$; 0.20 (0.21) at $x = 0.1$) in these two systems (Fig. 3d and Fig. 4d).

Although the three sorts of materials show similar Zn content dependencies of the electrical properties, Zn substitution in CIT alters the basic conducting mechanism, in that these materials have different carrier concentrations and mobilities (see Tables 3 and 4). In the CI-poor samples, the p-type carrier concentrations are high, as a large number of $Zn_{In}^-$ anti-site defects and $V_{Cu}^-$ copper vacancies are formed as acceptors, even though there are small quantities of $Zn_{Cu}^+$ and $In_{Cu}^{2+}$, which tend to cancel the p-type carriers to some degree. In this regard, the negative effect of the increased $n$ values on the Seebeck coefficients seems to be cancelled by the large effective masses ($m^*$ = 1.03–1.09) in the CI-poor samples. However, in the In-poor samples, the situation has changed. In spite of the fact that the carrier concentrations are not high, due to an increase in the number of $In_{Cu}^{2+}$ donor defects and a limited number of p-type $V_{Cu}^-$ copper vacancies, the effective masses, $m^*$, are low compared to those in the CI-poor counterparts, hence the $\alpha$ values are still comparable to those of the CI-poor samples (Fig. 3a). In the Cu-poor samples, there are large quantities of $Zn_{In}^-$ and $V_{Cu}^-$ acceptors due to the Cu deficiency, but there is a certain concentration of $Zn_{Cu}^+$ and a significantly increased concentration of $In_{Cu}^{2+}$.

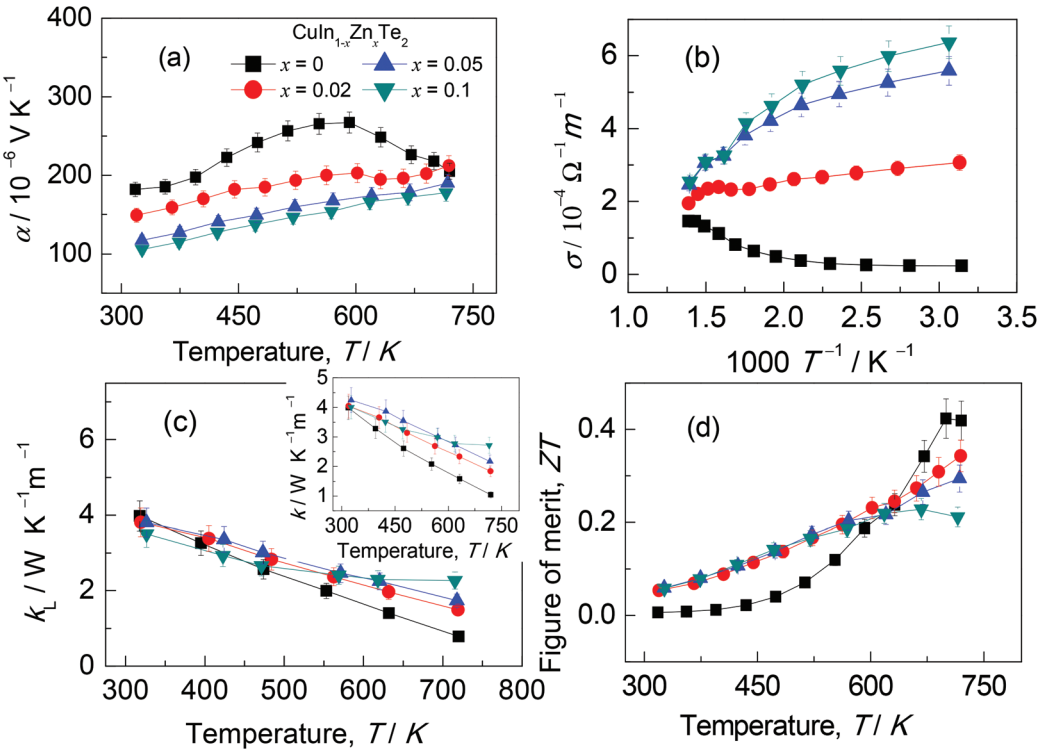


**Fig. 3** Thermoelectric properties of $CuIn_{1-x}Zn_xTe_2$: (a) Seebeck coefficients ($\alpha$), (b) electrical conductivities ($\sigma$), (c) lattice thermal conductivities ($\kappa_L$) (the inset shows the relationship between $\kappa$ and $T$), and (d) $ZT$ values.

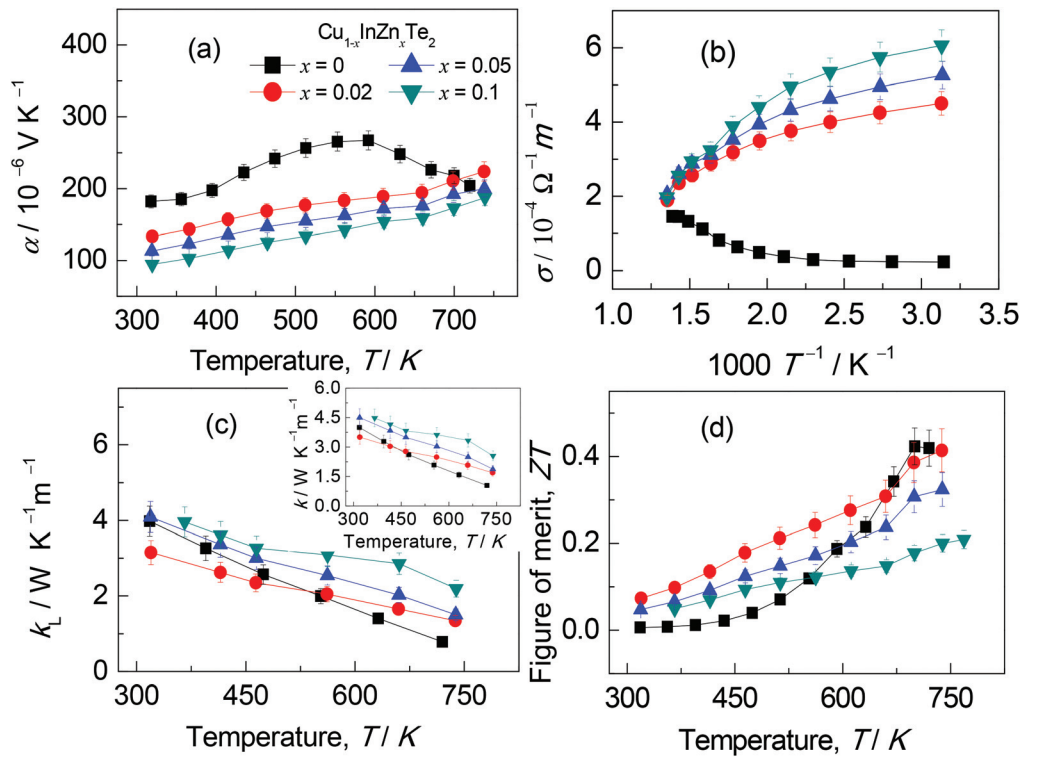


**Fig. 4** Thermoelectric properties of $Cu_{1-x}InZn_xTe_2$: (a) Seebeck coefficients ($\alpha$), (b) electrical conductivities ($\sigma$), (c) lattice thermal conductivities ($\kappa_L$) (the inset shows the relationship between $\kappa$ and $T$), and (d) $ZT$ values.

Therefore, the total carrier concentration, $n$, in the Cu-poor samples shows a tendency to decrease (Table 4). Because the effective masses, $m^*$, (0.32 at $x$ = 0.02; 0.17 at $x$ = 0.1) are not high, the Cu-poor systems do not have higher $\alpha$ values (Fig. 4a). Likewise, the electrical conductivity also bears little relation to the chemical composition (Fig. 3 and 4a and b), because the $\sigma$ values are simultaneously governed by two competing parameters, $n$ and $\mu$ (Table 4).

In CIT and the chalcopyrites based on CIT, the cation–anion bond lengths were determined to be 0.26–0.28 nm using Rietveld refinements, which is comparable to the size of the mean free path of phonons in solids (~0.3 nm).[29] In light of this, any tiny adjustment of the crystal distortion will alter the phonon scattering mechanism, changing the lattice conductivity ($\kappa_L$) at high temperatures.[4] On the other hand, the parameters $u$ ($\eta$), representing the anion position displacements in the chalcopyrites,[3b,30] show a tendency to increase (decrease) with increasing Zn content, and all approach the equilibrium values ($u$ = 0.25, $\eta$ = 1)[3b] (Table 4). This suggests that the lattice distortion is diminished, which accounts for the enhancement of $\kappa_L$. To further confirm this, we calculated the $d_{(Cu–Te)4a}$ and $d_{(In–Te)4b}$ bond lengths using Rietveld refinements with the parameters shown in Table 1. The results are shown in Fig. 5, in which we observed that the $d_{(Cu–Te)4a}$ bond length exhibits a tendency to increase linearly, while the $d_{(In–Te)4b}$ bond length shows a tendency to decrease with increasing Zn content. These results clearly reveal that the bond length difference ($\Delta d$) between Cu–Te and In–Te is gradually reduced, thus clarifying the diminution of the lattice distortion.

On the other hand, the lattice conductivity, $\kappa_L$, has a direct correlation with the phonon relaxation time, $\tau$, which mainly consists of point defects ($\tau_D$), phase/grain boundaries ($\tau_B$), Umklapp ($\tau_U$) and normal processes ($\tau_N$),[31] which gives:

$$\tau^{-1} = \tau_D{}^{-1} + \tau_B{}^{-1} + \tau_U{}^{-1} + \tau_N{}^{-1} \quad (13)$$

However, we only need to concentrate on the point defects ($\tau_D$) in the present material systems, as these three sorts of materials have similar $\tau_B$, $\tau_U$ and $\tau_N$. In the CI-poor system, the number of p-type defects increases upon Zn substitution, which thereby tends to significantly reduce the $\tau_D$ and $\kappa_L$ values at high temperatures. While in the Cu(In)-poor systems, the number of p-type carriers shows a tendency to decrease, therefore the $\tau_D$ values tend to increase. This is why we have observed relatively high $\kappa_L$ values.

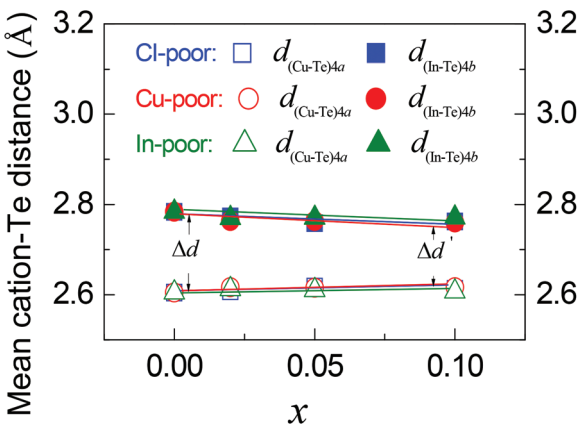


Fig. 5 Zn content ($x$) *versus* the mean cation–Te distance derived from Rietveld refinements for an X-ray powder diffraction experiment.

## 4. Conclusions

Upon Zn substitution in $CuInTe_2$, we observed multiple polyanionic/polycationic anti-site defects ($Zn_{In}^-$, $V_{Cu}^-$, $In_{Cu}^{2+}$ and/or $Zn_{Cu}^+$), each of which makes its own contribution to the band structure and transport properties. In general, Zn substitution in $CuInTe_2$ alters the basic conducting mechanism, but both the Seebeck coefficient and the electrical conductivity bear little relation to the Zn content. The lattice thermal conductivity ($\kappa_L$) is enhanced with increasing Zn content due to diminished lattice distortion, which is confirmed by the reduced bond length difference ($\Delta d$) between $d_{(Cu–Te)4a}$ and $d_{(In–Te)4b}$ and the gradually increasing anion position displacement, $u$. The CI-poor sample ($x$ = 0.02) has a higher lattice distortion and a lower $\kappa_L$ compared to its Cu(In)-poor counterparts. We attained the highest $ZT$ value of 0.69 at 737 K, which is an increase by a factor of 1.65 compared with Zn-free CIT.

## Acknowledgements

This work is supported by the National Natural Science Foundation of China (51171084 and 50871056), Zhejiang Provincial Natural Science Foundation (LY14E010003), Ningbo International Cooperation Project (2011D10012), and Ningbo Natural Science Foundation (2014A610016). We should also acknowledge the band structure calculations by Dr W.H. Fan from Taiyuan University of Technology, Taiyuan, China.

## References

1 (*a*) T. Plirdpring, K. Kurosaki, A. Kosuga, T. Day, S. Firdosy, V. Ravi, G. J. Snyder, A. Harnwunggmoung, T. Sugahara, Y. Ohishi, H. Mut and S. Yamanaka, *Adv. Mater.*, 2012, **24**, 3622; (*b*) R. L. Liu, H. L. Xi, H. L. Liu, X. Shi, W. Q. Zhang and L. D. Chen, *Chem. Commun.*, 2012, **48**, 3818; (*c*) A. Yusufu, K. Kurosaki, A. Kosuga, T. Sugahara, Y. Ohishi, H. Muta and S. Yamanaka, *Appl. Phys. Lett.*, 2011, **99**, 061902; (*d*) A. Kosuga, T. Plirdpring, R. Higashine, M. Matsuzawa, K. Kurosaki and S. Yamanaka, *Appl. Phys. Lett.*, 2012, **100**, 042108; (*e*) Y. P. Li, Q. S. Meng, Y. Deng, H. Zhou, Y. L. Gao, Y. Y. Li, J. F. Yang and J. L. Cui, *Appl. Phys. Lett.*, 2012, **100**, 231903; (*f*) N. Cheng, R. Liu, S. Bai, X. Shi and L. Chen, *J. Appl. Phys.*, 2014, **115**, 163705.

2 (*a*) P. Prabukanthan and R. Dhanasekaran, *Mater. Res. Bull.*, 2008, **43**, 1996; (*b*) I. V. Bodnar, A. Eifler, T. Doering,

W. Schmitz, K. Bente, V. F. Gremenok, I. A. Victorov and V. Riede, *Cryst. Res. Technol.*, 2000, **35**, 1135; (*c*) M. J. Thwaites, R. D. Tomlinson and M. J. Hampshire, *Inst. Phys. Conf. Ser.*, 1997, **35**, 237.

3 (*a*) J. E. Jaffe and A. Zunger, *Phys. Rev. B*, 1983, **28**, 5822; (*b*) J. E. Jaffe and A. Zunger, *Phys. Rev. B*, 1984, **29**, 1882; (*c*) J. Zhang, R. Liu, N. Cheng, Y. Zhang, J. Yang, C. Uher, X. Shi, L. Chen and W. Zhang, *Adv. Mater.*, 2014, **26**, 3848.

4 (*a*) W. C. Wu, Y. P. Li, Z. L. Du, Q. S. Meng, Z. Sun, W. Ren and J. L. Cui, *Appl. Phys. Lett.*, 2013, **103**, 011905; (*b*) J. L. Cui, Y. P. Li, Z. L. Du, Q. S. Meng and H. Zhou, *J. Mater. Chem. A*, 2013, **1**, 677.

5 S. B. Zhang, S. H. Wei and A. Zunger, *Phys. Rev. Lett.*, 1997, **78**, 4059.

6 Y. J. Zhao and A. J. Freeman, *J. Magn. Magn. Mater.*, 2002, **246**, 145.

7 L. J. Lin, J. H. Wernick, N. Tabatabaie, G. W. Hull and B. Meagher, *Appl. Phys. Lett.*, 1987, **51**, 2051.

8 J. L. Yao, Z. X. Wang, J. V. Tol, N. S. Dalal and J. A. Aitken, *Chem. Mater.*, 2010, **22**, 1647.

9 Y. J. Zhao and A. Zunger, *Phys. Rev. B: Condens. Matter Mater. Phys.*, 2004, **69**, 075208.

10 J. L. Yao, N. J. Takas, M. L. Schliefert, D. S. Paprocki, P. E. R. Blanchard, H. Y. Gou and A. Mar, *Phys. Rev. B: Condens. Matter Mater. Phys.*, 2011, **84**, 075203.

11 S. B. Zhang, S. H. Wei and A. Zunger, *Phys. Rev. B: Condens. Matter*, 1998, **57**, 9642.

12 W. Shan, W. Walukiewicz, J. W. Ager III and E. E. Haller, *Phys. Rev. Lett.*, 1999, **82**, 1221.

13 K. S. Liang, A. Bienenstock and C. W. Bates, *Phys. Rev. B: Solid State*, 1974, **10**, 1528.

14 W. Shan, W. Walukiewicz, J. W. Ager III, K. M. Yu, J. Wu, E. E. Haller, Y. Nabetani, T. Mukawa, Y. Ito and T. Matsumoto, *Appl. Phys. Lett.*, 2003, **83**, 299.

15 J. H. Lee, J. Q. Wu and J. C. Grossman, *Phys. Rev. Lett.*, 2010, **104**, 016602.

16 L. Roussak, G. Wagner, S. Schorr and K. Bente, *J. Solid State Chem.*, 2005, **178**, 3476.

17 T. Colakoğlu and M. Parlak, *Appl. Surf. Sci.*, 2008, **254**, 1569.

18 M. D. Segall, P. J. D. Lindan, M. J. Probert, C. J. Pickard, P. J. Hasnip, S. J. Clark and M. C. Payne, *J. Phys.: Condens. Matter*, 2002, **14**, 2717.

19 J. P. Perdew, K. Burke and M. Ernzerhof, *Phys. Rev. Lett.*, 1996, **77**, 3865.

20 S. H. Wei, S. B. Zhang and A. Zunger, *Appl. Phys. Lett.*, 1998, **72**, 3199.

21 J. F. Moulder and J. Chastain, *Handbook of X-ray Photoelectron Spectroscopy: A Reference Book of Standard Spectra for Identification and Interpretation of XPS Data*, Perkin-Elmer Corporation: Physical Electronics Division, Eden Prairie, Minnesota, 1992, pp. 261.

22 (*a*) R. P. Vasquez, *Surf. Sci. Spectra*, 1993, **2**, 144; (*b*) R. P. Vasquez, *Surf. Sci. Spectra*, 1993, **2**, 149.

23 S. M. Wasim, C. Rincón, G. Marín and J. M. Delgado, *Appl. Phys. Lett.*, 2000, **77**, 94.

24 G. J. Snyder and E. S. Toberer, *Nat. Mater.*, 2008, **7**, 105.

25 N. Tsujii and T. Mori, *Appl. Phys. Express*, 2013, **6**, 043001.

26 E. S. Toberer, A. F. May and G. J. Snyder, *Chem. Mater.*, 2010, **22**, 624.

27 (*a*) Y. Pei, H. Wang and G. J. Snyder, *Adv. Mater.*, 2012, **24**, 6125; (*b*) A. F. Ioffe, *Semiconductor Thermoelements, and Thermoelectric Cooling*, Infosearch, London, 1957; (*c*) Y. Pei, A. D. LaLonde, N. A. Heinz, X. Shi, S. Iwanaga, H. Wang, L. Chen and G. J. Snyder, *Adv. Mater.*, 2011, **23**, 5674; (*d*) A. J. Crocker and L. M. Rogers, *J. Phys. Colloq.*, 1968, **29**, C4-129; (*e*) L. M. Rogers and A. J. Crocker, *J. Phys. D: Appl. Phys.*, 1971, **4**, 1016; (*f*) A. J. Crocker and B. J. Sealy, *J. Phys. Chem. Solids*, 1972, **33**, 2183; (*g*) L. Rogers and A. Crocker, *J. Phys. D: Appl. Phys.*, 1972, **5**, 1671.

28 (*a*) J. L. Cui, X. J. Zhang, Y. Deng, H. Fu, Y. M. Yan, Y. L. Gao and Y. Y. Li, *Scr. Mater.*, 2011, **64**, 510; (*b*) J. L. Cui, X. L. Liu, X. J. Zhang, Y. Y. Li and Y. Deng, *J. Appl. Phys.*, 2011, **110**, 023708.

29 R. Berman, *Thermal Conduction in Solids*, Clarendon Press, Oxford University, 1976.

30 (*a*) S. C. Abrahams and J. L. Bernstein, *J. Chem. Phys.*, 1973, **59**, 5415; (*b*) S. C. Abrahams and J. L. Bernstein, *J. Chem. Phys.*, 1974, **61**, 1140.

31 (*a*) Y. Luo, J. Yang, G. Li, M. Liu, Y. Xiao, L. Fu, W. Li, P. Zhu, J. Peng, S. Gao and J. Zhang, *Adv. Energy Mater.*, 2014, **4**, 1300599; (*b*) M. Liu and X. Y. Qin, *Appl. Phys. Lett.*, 2012, **101**, 132103; (*c*) M. Liu, X. Y. Qin, C. S. Liu and Z. Zeng, *Appl. Phys. Lett.*, 2011, **99**, 062112; (*d*) H. Y. Lv, H. J. Liu, X. J. Tan, L. Pan, Y. W. Wen, J. Shi and X. F. Tang, *Nanoscale*, 2012, **4**, 511; (*e*) J. He, S. N. Girard, M. G. Kanatzidis and V. P. Dravid, *Adv. Funct. Mater.*, 2010, **20**, 764.

 